Direct verification of the lubrication force on a sphere travelling through a viscous film upon approach to a solid wall

J. O. MARSTON[1,3]†, W. YONG[2] AND S. T. THORODDSEN[3]

[1]A-STAR Institute of Chemical and Engineering Sciences, 1 Pesek Road, Jurong Island,
Singapore 627833

[2]Department of Chemical and Biomolecular Engineering, National University of Singapore,
4 Engineering Drive 4, Singapore 117576

[3]Division of Physical Sciences and Engineering, King Abdullah University of Science and Technology,
Thuwal 23955-6900, Saudi Arabia

Experiments were performed to observe the motion of a solid sphere approaching a solid wall through a thin layer of a viscous liquid. We focus mainly on cases where the ratio of the film thickness, δ, to the sphere diameter, D, is in the range $0.03 < \delta/D < 0.09$ and the Stokes number, St, a measure of the sphere inertia to viscous forces, is below a critical level St_c so that the spheres do not rebound and escape from the liquid layer. This provides us with the scope to verify the force acting on the sphere, derived from lubrication theory. Using high-speed video imaging we show, for the first time, that the equations of motion based on the lubrication approximation correctly describe the deceleration of the sphere when $St < St_c$. Furthermore, we show that the penetration depth at which the sphere motion is first arrested by the viscous force, which decreases with increasing Stokes number, matches well with theoretical predictions. An example for a shear-thinning liquid is also presented, showing that this simple set-up may be used to deduce the short-time dynamical behaviour of non-Newtonian liquids.

1. Introduction

When a sphere is in close approach to a wall perpendicular to the motion (see figure 1*a*), the Stokes force acting on the sphere, $F_\mu = 6\pi\mu a v$, where μ is the fluid dynamic viscosity, a is the sphere radius and v is the sphere velocity (see e.g. Brenner 1961) is corrected by a factor of a/x where x is the separation distance between the nose (i.e. south pole) of the sphere and the wall, so that the lubrication force exerted on the sphere is given by

$$F_L = 6\pi\mu a^2 v/x. \tag{1.1}$$

This correction factor has been experimentally examined by Ambari, Gauthier-Manuel & Guyon (1984) by translating a solid wall towards a sphere levitated in a cylindrical tube filled with silicone oil. In their experiments, the translation velocities were of the order $10^{-5}\,\mathrm{m\,s^{-1}}$ and the sphere was fully immersed in the fluid. This lubrication force is the force responsible for the deformation of the sphere

† Email address for correspondence: jeremy.marston@kaust.edu.sa

once the separation distance, x, becomes comparable to an elasticity length scale, $x_r = (3\pi\theta\mu a^{3/2} v_0/\sqrt{2})^{2/5}$ (Davis, Rager & Good 2002), where v_0 is the sphere velocity at the initial separation x_0, $\theta = (1 - v_1^2)/\pi E_1 + (1 - v_2^2)/\pi E_2$, v_1 and v_2 are the Poisson's ratios of the sphere and plane and E_1 and E_2 are the Young's modulus of the sphere and plane. Note that this scaling only holds if the sphere retains half of its initial velocity, that is $v = v_0/2$ at $x = x_r$. If the deformation of the solid is significant, rebound may occur as the elastic strain energy is converted back to kinetic energy. This process is at the core of inter-particle and particle-wall collisions which are a fundamental physical phenomenon and ubiquitous in many industrial processes. The nature of the impacts can vary widely, from wet and dry particle collisions during a granulation process (Salman, Hounslow & Seville 2006) to immersed particle collisions during sedimentation and filtration.

In attempt to elucidate some of the features of a wet collision, several ideal problems have previously been considered; a spherical particle impacting another spherical particle or a plane immersed in a liquid (Davis, Serayssol & Hinch 1986; Lian, Adams & Thornton 1996; Gondret, Lance & Petit 2002), a dry spherical particle impacting a wet surface (Barnocky & Davis 1988; Davis *et al.* 2002) and wet spherical particles colliding in air (Donahue *et al.* 2009). Though not entirely representative of a typical impact or collision in applications such as granulation, these problems reveal some wonderful insight into the physics occurring in such applications.

The first authoritative work by Davis *et al.* (1986) revealed two main dimensionless parameters, namely the Stokes number and an elasticity parameter:

$$St = \frac{\rho_s D v_o}{9\mu}, \quad \epsilon = 4\theta\mu v_o a^{3/2}/x_0^{5/2}, \quad (1.2)$$

where ρ_s and D are the density and diameter of the solid sphere. Their work showed that no rebound occurs when the Stokes number is below a critical value, i.e. when $St < St_c$ and was verified by Barnocky & Davis (1988). The critical Stokes number has been expressed as a function of the elasticity parameter given as $St_c = 0.52\ln(1/\epsilon) - 1.67$ by Lian *et al.* (1996) or, similarly, $St_c = 0.4\ln(1/\epsilon) - 0.2$ by Davis *et al.* (2002). Other configurations have also confirmed the presence of a critical value of the Stokes number during elastohydrodynamic collisions (Gondret *et al.* 1999; Gondret *et al.* 2002). Some recent works (e.g. Kantak, Hrenya & Davis 2009) have incorporated the original elastohydrodynamic theory to investigate multi-particle systems. Davis *et al.* (2002) performed measurements of the coefficient of restitution (i.e. the ratio of the rebound velocity to the impact velocity) using a stroboscope with a temporal resolution of 0.01 s. However, none of the above works observe the actual short-time dynamics of the sphere as it first penetrates the liquid. This observation has now become feasible due to recent advances in high-speed video imaging (Thoroddsen, Etoh & Takehara 2008).

As such, we revisit the elastohydrodynamic problem with the purpose of providing a direct verification of the lubrication force (1.1) during the short-time ($t \leqslant 20\,\text{ms}$) dynamics of the sphere upon close approach to a wall where the wall is covered with a thin film of viscous liquid ($\delta/D \ll 1$). The observations of close approach from the high-speed imaging are compared directly to the equations of motion which account only for the viscous lubrication and sphere inertia. Both the separation distance and the time at which the sphere is first arrested agree well with the theory assuming zero solids deformation for a Newtonian liquid. It is thus shown that the elasticity length scale and the Stokes number are the correct fitting
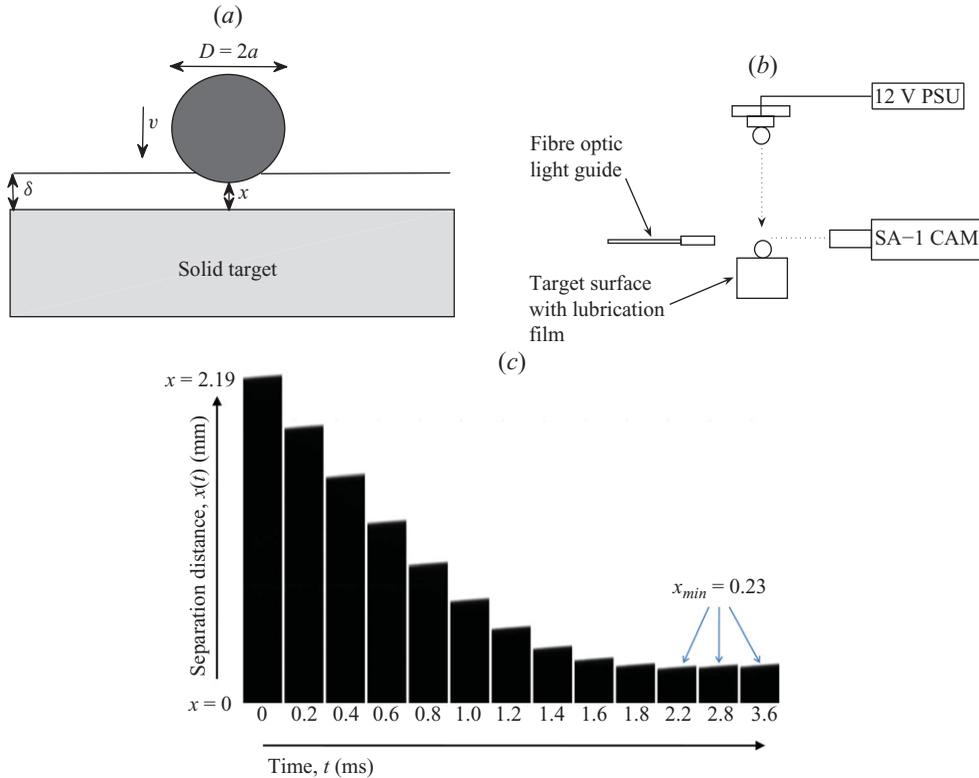
FIGURE 1. (*a*) Sketch showing the physical parameters in the close approach of a sphere towards a wall. (*b*) Schematic of the experimental set-up used. (*c*) Example of raw data from a video sequence taken for the impact of a $D = 50$ mm sphere onto a $\delta = 2.25$ mm film of pure syrup at $u_i = 1.59$ m s^{-1}. The first panel shown is taken just after entry into the film with $x = 2.19$ mm and subsequent frames are taken at time $t = 0.2, 0.4, 0.6, 0.8, 1, 1.2, 1.4, 1.6, 1.8, 2.2, 2.8, 3.6$ ms. In the final panel, $x = 230$ μm.

parameters for the data. We also present data for a specific case where the fluid is strongly non-Newtonian showing strong deviations from the classical description of motion.

2. Materials and Methods

In the experiments, a stainless steel sphere, $D = 25, 38$ or 50 mm, is released from an electromagnetic holder suspended directly above the liquid layer. The liquid film is contained within a marked perimeter on the target surface. Two target surfaces were considered in these experiments, namely glass and steel. Both targets were solid blocks with dimensions 0.11 m $\times 0.11$ m $\times 0.065$ m and were placed directly on a ground-level concrete floor to ensure the target remained rigid throughout the impact. Liquid films with thickness $\delta = 1.15, 2.3$ and 3.45 mm were examined. For the steel onto glass impact $\theta \sim 6.15 \times 10^{-12}$ and $\epsilon \sim 10^{-5} - 10^{-3}$ and the corresponding values for steel onto steel are $\theta \sim 2.87 \times 10^{-12}$ and $\epsilon \sim 10^{-6} - 10^{-4}$ in these experiments. A schematic of the experimental set-up used is shown in figure 1(*b*).

The apex of the sphere is tracked using a Photron Fastcam SA1 high-speed camera at a frame rate of 50 Kfps which yields a resolution of 64×736 pixels and a
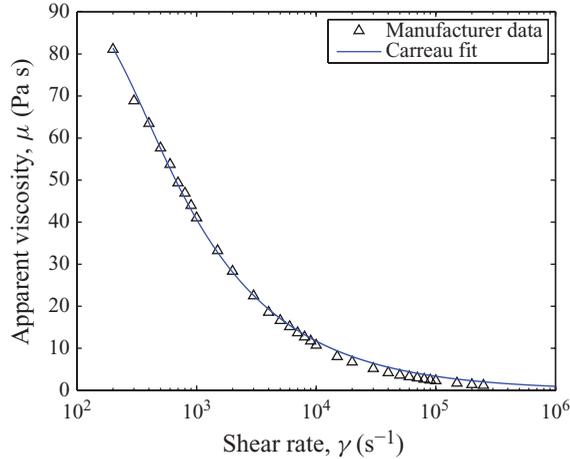
FIGURE 2. Rheological data for 100 000 cSt silicone oil. The data points are taken from the manufacturer's data and the theoretical fit with the Carreau model assumes a zero shear $\mu_0 = 97.7$ Pa s (as stated by the manufacturer). The resulting parameters are $\mu_\infty = 0$, $\lambda = 4.88 \times 10^{-3}$ and $n = 0.455$.

recording time long enough to allow for manual triggering of the video sequence. Backlighting is provided by a single fibre-optic guide attached to a 350 W Sumita Metal Halide light source. Using a Leica Z16 long-distance microscope at $4 - 6.3 \times$ optical magnification, the effective pixel resolution is in the range $3.3 - 5.06$ μm pixel^{-1} which, given the high contrast of the images, yields high accuracy in the measurement of the separation distance between the tip of the sphere and the wall surface. An example of the raw data format is given in figure 1(c). Here, the top of the black strip marks the apex of the sphere from which we deduce the effective separation distance $x(t)$, so that the bottom of the strips indicates a zero separation distance, $x = 0$ (i.e. physical contact with the plate). For this example, the minimum distance is $x_{min} = 230$ μm.

The apex is tracked from the instant it enters the top of the frame with effective time steps of $\Delta t = 20$ μs. For the initial motion and deceleration of the sphere, only the first ~ 1000 frames ($t = 0.02$ s) from the video clips are analysed using an image correlation routine in Matlab.

For comparison to theory, we use pure Tate & Lyle's Golden Syrup for it's high viscosity and strictly Newtonian behaviour, however, dilute mixtures (in water) to examine the effect of viscosity were also used. The entire experimental facility was placed in a humidity chamber to eliminate viscosity changes through moisture absorption. However, due to minor temperature fluctuations between 21°C and 23°C the viscosity of the syrup was measured every 0.5°C with an Anton Paar MCR301 Rheometer with concentric cylinder geometry, with resulting viscosities 25.5, 27.5, 29.7, 31 and 34.6 Pa s. For the non-Newtonian case examined here, we used (dimethylpolysiloxane) Silicone oil (Shin-Etsu Chemical Co. Ltd, Japan) with low-shear kinematic viscosity $\nu = 100\,000$ cSt ($\mu = 97.7$ Pa s). These fluids are known to be highly shear-thinning and compressible. The rheological data for this fluid can be seen in figure 2 where the data points are taken from the manufacturer's data and the theoretical fit is provided by the Carreau model $(\mu - \mu_\infty)/(\mu_0 - \mu_\infty) = [1 + (\lambda \dot{\gamma})^2]^{(n-1)/2}$ with $\mu_0 = 97.7$ Pa s, $\mu_\infty = 0$, $\lambda = 4.88 \times 10^{-3}$ s and $n = 0.455$.

3. Results and discussion

In figures 3(a), 3(c) and 3(e) we show examples of data for separation distance versus time, velocity versus separation distance and lubrication force versus separation distance, respectively. The raw data (figure 3a) was obtained directly from the high-speed video sequences in a series of experiments for a $D = 50$ mm sphere impacting onto a $\delta = 2.25$ mm film of pure golden syrup ($\mu = 29.6$ Pa s) for several impact velocities $u_i = 0.53$, 0.83, 1.18, 1.42, 1.73 and 1.92 m s^{-1} measured from just prior to the sphere entering the thin film. Note that $St < St_c$ for all impact velocities here (see figure caption for values). Figure 3(a) for the separation distance versus time (from 1000 frames) shows that the motion is largely arrested by $t = 5$ ms. As expected, the penetration depth increases monotonically with sphere impact velocity. The data in figure 3(c) is derived directly from figure 3(a) and is plotted from $x = x_0 = 2\delta/3$. The data shows the decay of the velocity from $v = v_0$ at $x = x_0$ to $v = 0$ at $x = x_{min}$, i.e. the point at which the experimental velocity of the sphere first reaches zero. Although the sphere has not reached a true equilibrium level (evident from figure 3(a)), based on the threshold used to derive the raw data in figure 3(a) and limited resolution, the velocity has effectively reached zero by $t = 5$ ms for the data shown. This corresponds to the lubrication force having become negligible and further motion is simply the asymptotic settling of the sphere under the action of gravity (note that for perfectly smooth surfaces, an effectively infinite time would be required for physical contact to occur (Cox & Brenner 1967), however, in practice roughness of the materials, typically $O(10^{-6})$m, may induce physical contact at finite times). We can make use of this fact in order to deduce an effective minimum distance to compare to theoretical predictions for the closet approach, discussed later. The solid lines in figure 3(c) are derived from equation (8) of Davis *et al.* (1986), i.e.

$$v/v_0 = 1 - \ln(x/x_0)/St, \tag{3.1}$$

and generally provide a good qualitative description of the behaviour, but slightly overestimate the penetration depth for the higher impact velocities.

From figure 3(e) we see that the force (calculated from (1.1) using the data points from figure 3c) decays gradually for the lowest impact velocity, $u_i = 0.55$ m s^{-1}, but increases to a maximum before sharply falling to zero for all other impact velocities. This effect becomes more pronounced with the larger impact velocities and is understood by the fact that the separation distance diminishes faster than the impact velocity over the initial stages of penetration. Conversely, the sharp drop in force as $x \rightarrow x_{min}$ is due to the rapid decay in velocity. Figure 3(e) also includes theoretical predictions for the lubrication force, calculated from (1.1), shown by the solid lines and exhibiting reasonable agreement.

In contrast, in figures 3(b), 3(d) and 3(f) we show an equivalent set of data for a $D = 38$ mm sphere impacting a lower viscosity film of diluted (90 %) syrup with $\mu = 1.6$ Pa s. In this case, $St > St_c$ (see figure caption for values) and rebound occurs for all impact velocities ($u_i = 0.76$, 1.02, 1.34, 1.58 m s^{-1}) due to deformation of the sphere. In this case a definitive minimum level is observed in the data as a local minima in the separation distance – time curves, as shown in figure 3(b). Note for $u_i = 1.58$ m s^{-1}, the sphere leaves the field of view at $t = 6.8$ ms so no further data points could be taken. For $u_i = 0.76$, 1.02 and 1.34 m s^{-1}, the minimum separation distances reached are within 14 ± 8 μm of the solid surface where the error margin is based on 2 pixels needed to locate the interface. For $u_i = 1.58$ m s^{-1}, the experiments show several data points with $x < 0$ implying a strong deformation of the sphere
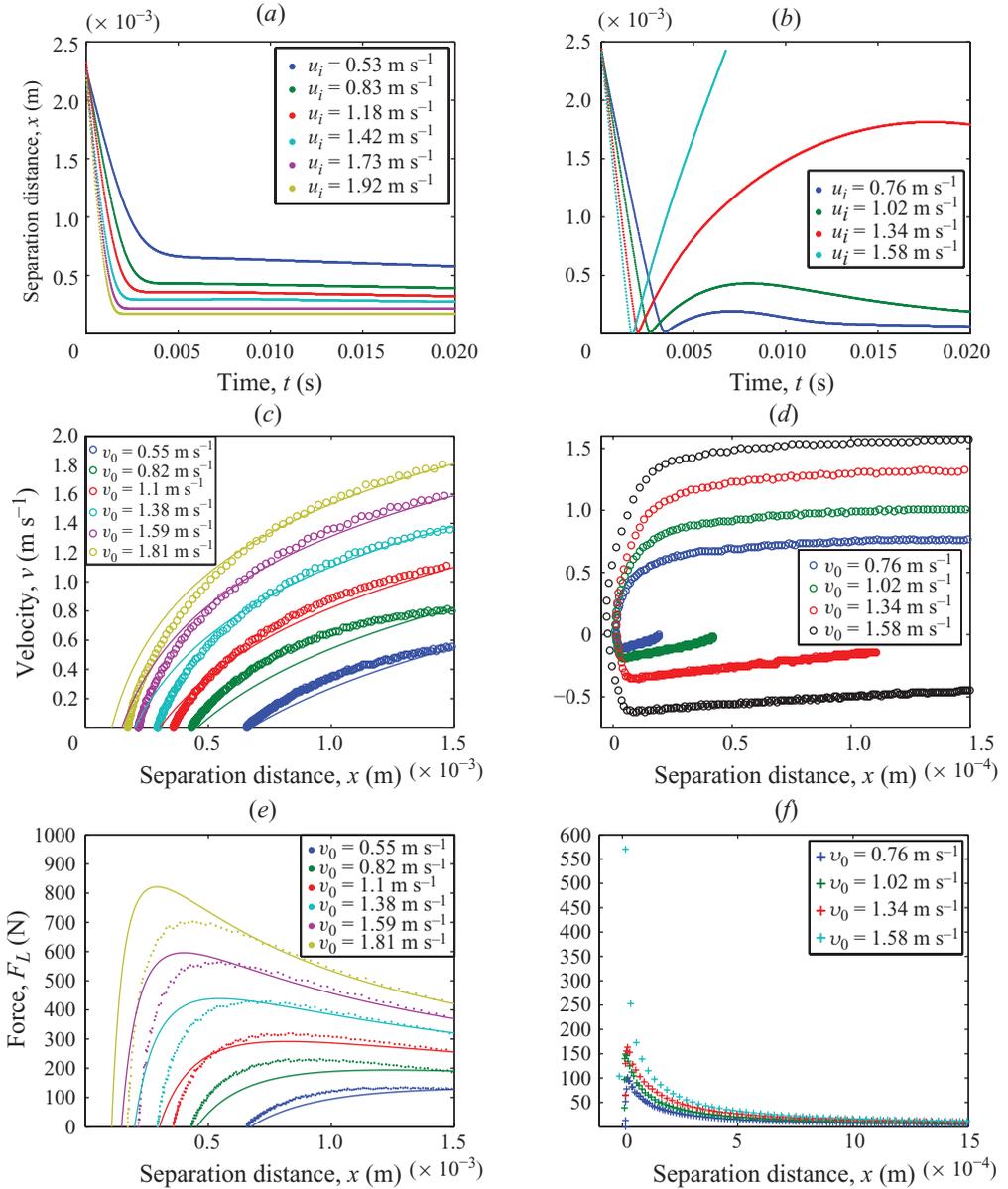
FIGURE 3. Plots of raw data for (a) separation distance versus time for $D = 50$ mm, $\delta = 2.25$ mm, pure syrup with $\mu = 29.6$ Pa s ($St = 0.8, 1.2, 1.6, 2.0, 2.3, 2.6$; $St_c = 4.2, 4.0, 3.9,$ $3.8, 3.7, 3.7$); (b) separation distance versus time for $D = 38$ mm, $\delta = 2.25$ mm, 90 % syrup with $\mu = 1.6$ Pa s ($St = 15.5, 20.8, 27.3, 32.2$; $St_c = 5.4, 5.3, 5.1, 5.1$); (c) velocity versus separation distance derived from (a); (d) velocity versus separation distance derived from (b); (e) force versus separation distance derived from (a); (f) force versus separation distance derived from (b). The solid lines in (c) and (e) represent the theoretical predictions from (3.1) and (1.1), respectively.

and possibly the substrate which is certainly supported by the strong rebound of the sphere out of the film.

Theoretically, the minimum separation distance can be predicted by the elasticity length scale x_r (Davis *et al.* 2002) which, for the parameters for figure 3(*b*) yields values of 5.8–7.8 μm, in reasonable agreement with the experimental values. Note, however, that the definition of x_r uses the approximation of $v^* = v_0/2$ for the velocity of the sphere, whereas here we can make a much better approximation by measuring the velocity just prior to rebound directly; Performing this measurement yields close approach velocities, $v^* = 0.4$, 0.45, 0.72 and 1.16 m s^{-1} respectively and the modified length scale, $x_{min} = (6\pi\theta\mu a^{3/2} v^*/\sqrt{2})^{2/5}$ predicts minimum separation distances of 8.4–12.9 μm.

In figure 3(*d*) we plot the velocity versus separation distance for this data including negative values of v in the rebound stage (c.f. figures 2 and 5 of Lian *et al.* 1996). These curves also show a much more rapid decay of the velocity as the sphere approaches the wall yielding the sharp peaks in figure 3(*f*) for the lubrication force, where only the positive values of F_L are shown as the theory becomes invalid during rebound due to effects of cavitation.

3.1. *Comparison to equations of motion*

Since data for the low viscosity films indicate strong deformation, we focus mainly on the realizations where $St < St_c$ to compare to the lubrication approximation (1.1). This comparison can be made by computing the velocity and force as a function of the separation distance, as seen in figures 3(*c*) and 3(*e*), however, a more straightforward comparison is made by simple numerical integration of the equations of motion (assuming no solid deformation) given by

$$\frac{\mathrm{d}x}{\mathrm{d}t} = -v, \quad m\frac{\mathrm{d}v}{\mathrm{d}t} = -F_L, \tag{3.2}$$

where $F_L(t)$, given by (1.1) is the viscous lubrication force acting on the sphere, $m = (4/3)\pi a^3 \rho_s$ is the mass of the sphere, $v = v(t)$ and $x = x(t)$ are the instantaneous velocity and separation distance. For the lubrication force to be valid, it is required that $x \ll a$, $\rho_l v x/\mu \ll 1$ and $\rho_l x/(\rho_s a) \ll 1$, where ρ_l is the liquid density. Typical parameters from the experimental study are $a = 0.025$ m, $x \leqslant 0.002$ m, $\rho_l = 1450$ kg m^{-3} (pure syrup), $v = O(1)$ m s^{-1}, $\mu = O(10)$ Pa s, $\rho_s = 7850$ kg m^{-3} (steel) so that all the above conditions are easily met. In accordance with Barnocky & Davis (1988), the calculations are started at $x_0 = 2\delta/3$ where δ is the film thickness. The initial velocities v_0 are provided directly from the video sequences.

As no solid deformation is assumed in this approximate model, the sphere will be arrested by the viscous force without rebound. This assumption is clearly valid for the higher viscosity experiments in figure 3(*a*). Also, following Barnocky & Davis (1988), we can approximate the dynamic capillary force acting on the sphere as $F_c \sim 4\pi a\sigma$ which, for a $D = 50$ mm sphere impacting pure syrup gives a value of $F_c = 0.025$ N, which is orders of magnitude smaller than the lubrication force throughout the impact phase so it can be neglected accordingly.

In figure 4(*a–h*), we present a direct comparison between the experimental data and the motion predicted by (3.2). Data for both the glass and steel targets is shown for pure syrup over a range of film thicknesses and sphere sizes (see captions for details). The results are plotted as separation distance versus time where the data has been scaled appropriately using the characteristic length x_0 and velocity v_0, starting at time t_0 (when the sphere passes through the level x_0). Since the model assumes no
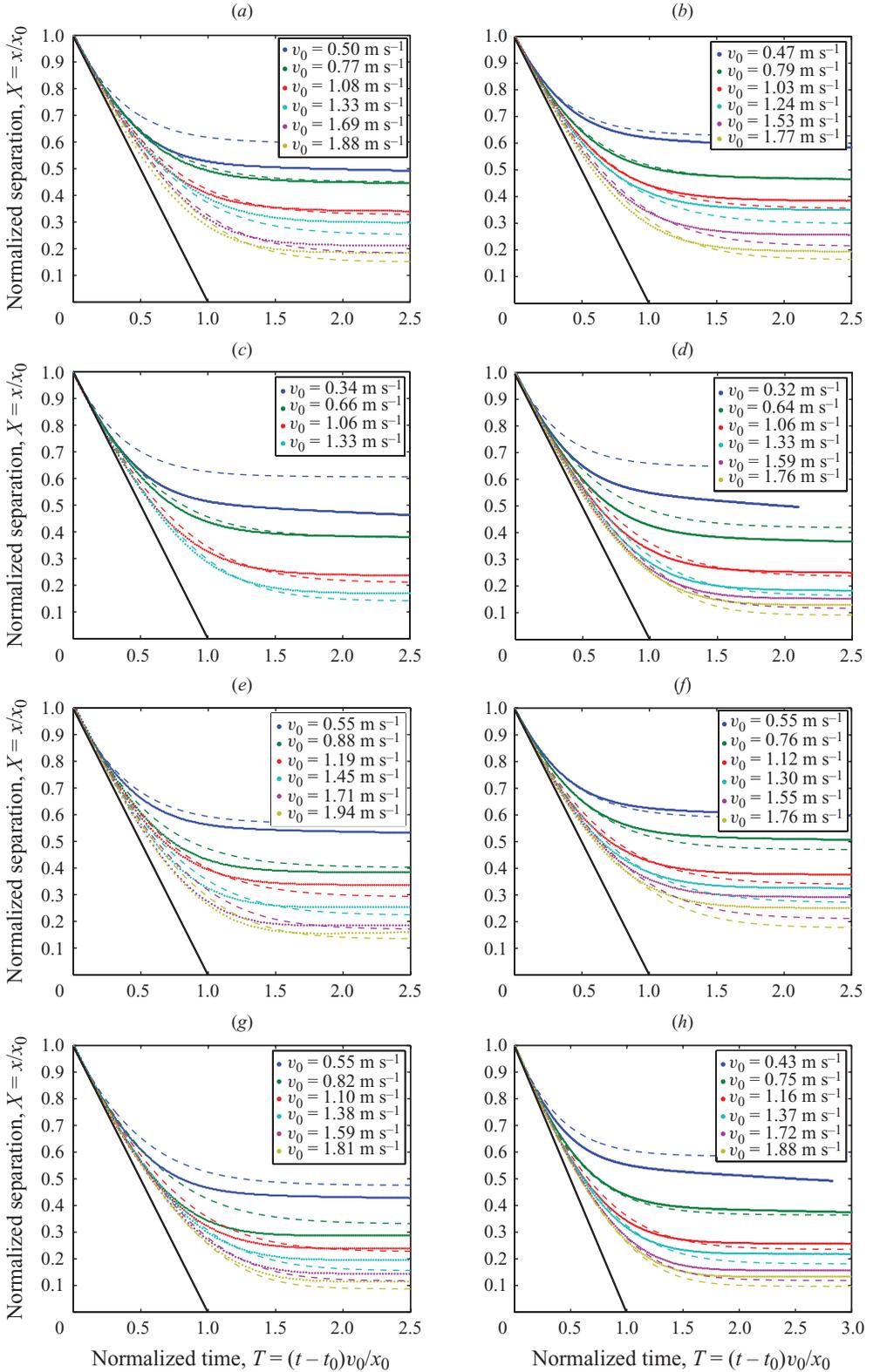
FIGURE 4. For legend see facing page.

deformation or rebound, the experimental data has only been plotted up to where the experimental velocity first reaches zero. The solid black lines in each plot represents motion for a constant velocity v_0 (i.e. no deceleration). It can be seen that the data is in good qualitative and quantitative agreement with the theory for most impact velocities and film thicknesses; however, we note that the theory underestimates the penetration for the lowest impact velocities (see e.g. figures 4d and 4h), which is due to gravitational settling in the experiments, and marginally overestimates the penetration for the higher impact velocities. To our knowledge, however, this data provides the first direct verification of the lubrication force (1.1) for a sphere travelling through a thin viscous film over a range of St and different substrates.

3.2. *Minimum separation distance*

To derive an experimental value for the minimum separation distance, x_{min}, we determine x at which the experimental velocity of the sphere first reaches zero (in practice, of course, the separation distance will gradually diminish due to the settling under gravity, but this settling is asymptotically slow and not observed over the duration of the video sequences here). As seen in figures 3(c) and 3(e), this corresponds to the stage at which the lubrication force has diminished sufficiently so that $F_L \leqslant mg$ and, as such, the lubrication force is no longer dominant in determining the motion of the sphere. Using this threshold, we can then make a quantitative comparison between the theory and experiment for the distance at which the viscous force effectively arrests the motion of the sphere. In figure 5, we plot the normalized distance of minimum separation, scaled with respect to the initial separation distance, $x_0 = 2\delta/3$, versus the impact Stokes number, $St = \rho_s D v_0/9\mu$.

As predicted by Davis *et al.* (1986) for the approach of two spheres, the data shows that the separation distance rapidly decreases as the Stokes number increases. An approximately four-fold increase in the Stokes number leads to a similar reduction in the scaled separation distance. Here, the theoretical values (dashed curves) are determined from the equations of motion (3.2) by defining x_{min} as the value of x at which $F_L \leqslant mg$. Applying this threshold for a range of St generates the curves shown. The rapid decrease of minimum approach with increasing Stokes number is expected due to the small values of the elasticity parameter ϵ and the data shows good agreement with the values predicted by the theory.

3.3. *Non-Newtonian films*

Experiments were also performed with certain non-Newtonian fluids with high nominal viscosities (measured at low shear rates) but with highly shear-thinning properties. Data for one such set of experiments is presented in figure 6(a) for silicone oil with low-shear viscosity of $\nu = 100\,000$ cSt ($\mu_0 = 97.7$ Pa s). The data shown is for a $D = 50$ mm sphere impacting a $\delta = 3.45$ mm film on a glass base. The data clearly indicates that for the higher impact velocities, $u_i = 1.22$, 1.41 and 1.69 m s^{-1}, the sphere

---

FIGURE 4. Comparison of sphere motion for (a) $D = 38$ mm, $\delta = 2.25$ mm, (b) $D = 38$ mm, $\delta = 3.45$ mm, (c) $D = 50$ mm, $\delta = 2.25$ mm, (d) $D = 50$ mm, $\delta = 3.45$ mm, (e) $D = 38$ mm, $\delta = 2.25$ mm, (f) $D = 38$ mm, $\delta = 3.45$ mm, (g) $D = 50$ mm, $\delta = 2.25$ mm, (h) $D = 50$ mm, $\delta = 3.45$ mm. In all cases the film is pure syrup and the target surface is steel for (a)–(d) and glass for (e)–(h). The dashed lines indicate the theoretical trajectories and the solid data points are those derived directly from the video sequences. Note that the theoretical trajectories and the experimental data begin at $x_0 = 2\delta/3$. The solid black lines indicate a slope of -1 which represents the trajectory with constant velocity v_0.
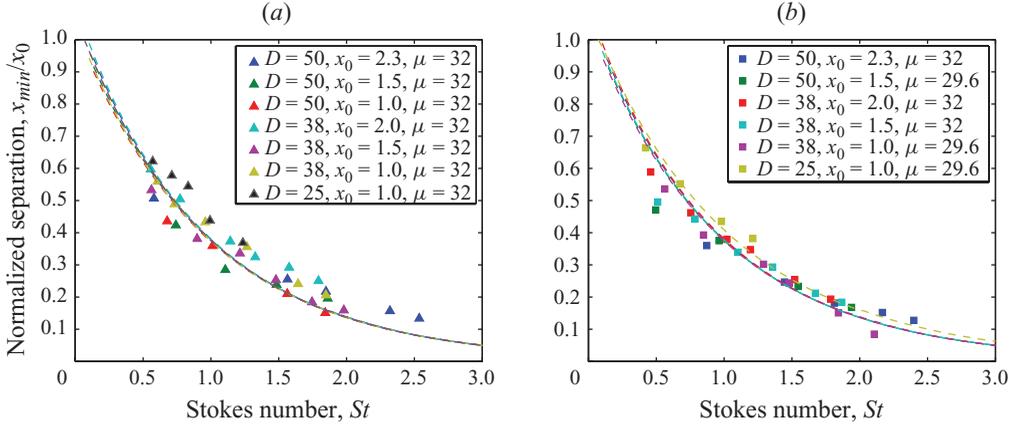
FIGURE 5. Minimum separation distances normalized by the initial separation, $x_0 = 2\delta/3$, plotted against the impact Stokes; number, $St = \rho_s D v_0/9\mu$, for (a) glass base and (b) steel base. The dashed lines indicate theoretical curves and data points are experimental values. Stated values of D are in mm, x_0 in mm and μ in Pa s.
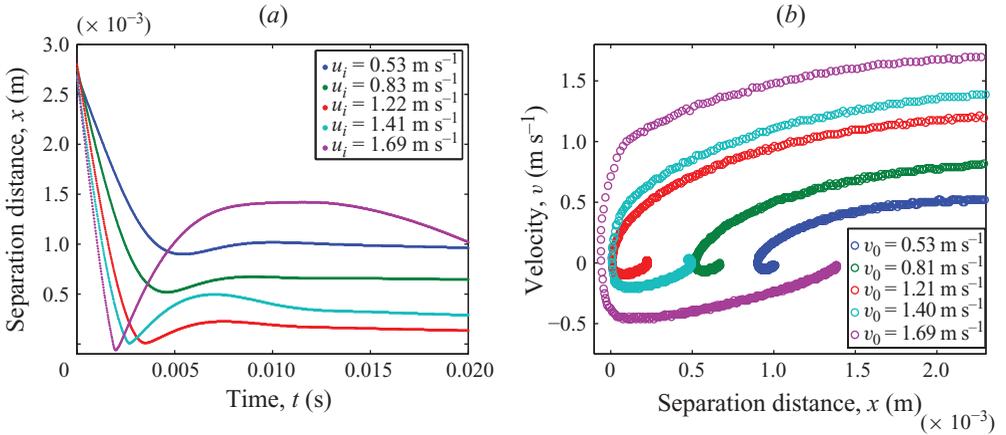
FIGURE 6. Raw data of (a) separation distance versus time and (b) velocity versus separation distance for a $D = 50$ mm sphere impacting a $\delta = 3.45$ mm film of $\nu = 100\,000$ cSt ($\mu_0 = 97.7$ Pa s) silicone oil which is non-Newtonian.

penetrates sufficiently deep into the film to cause deformation and rebound. Based on the nominal viscosity of this liquid, this is unexpected given that the values of the Stokes number, $St = 0.54$, 0.62 and 0.75, are much lower than the critical values of $St_c = 3.79$, 3.74 and 3.66. However, given that the film experiences shear, the reduction in effective viscosity during the impact leads to effective Stokes numbers, $St_{eff} = 4.06$, 4.69 and 5.67 (based on $\mu = 13$ Pa s, see later for details), whilst the critical values are $St_c = 4.61$, 4.55 and 4.47 showing that at least the two highest impact velocities are supercritical. More surprising is the fact that a slight apparent rebound is seen even for the two lowest impact velocities, $u_i = 0.53$ and $0.83\,\mathrm{m\,s^{-1}}$, where the sphere has clearly not penetrated deep enough into the layer to cause solid deformation. Note that these data points do meet the condition $\epsilon \ll 1$ and noting that $St_c > 1$, these cases do not fall into the category of rebound without deep penetration as outlined
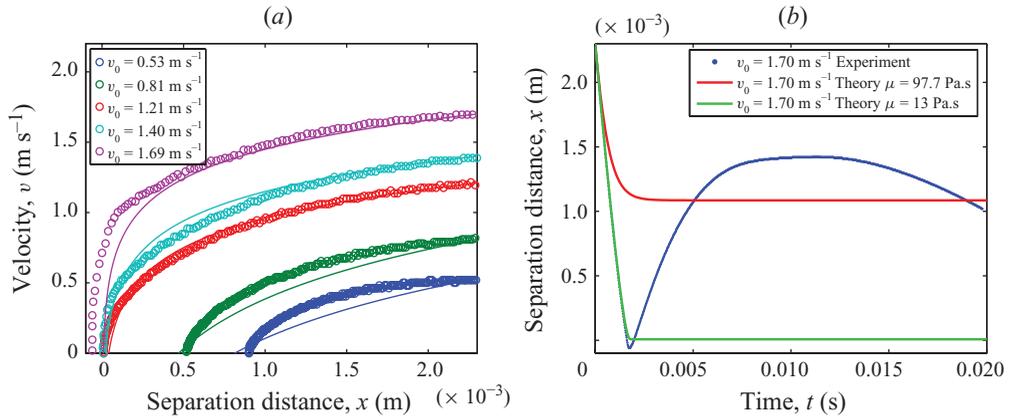
FIGURE 7. (a) Velocity versus Separation distance ($v(t) \geqslant 0$ only). Data is from figure 6(a) for a $D = 50$ mm sphere impacting a $\delta = 3.45$ mm film of $\nu = 100\,000$ cSt ($\mu_0 = 97.7$ Pa s) silicone oil. The solid lines are the best fits from (3.1) using single apparent viscosities of $\mu = 22$ Pa s for $u_i = 0.53$ and 0.81 m s^{-1} and $\mu = 13$ Pa s for $v_0 = 1.21$, 1.40 and 1.70 m s^{-1}. (b) Separation distance versus time for $D = 50$ mm, $v_0 = 1.70$ m s^{-1}, $\delta = 3.45$ mm and $\nu = 100\,000$ cSt ($\mu_0 = 97.7$ Pa s) silicone oil. The experimental data is from figure 5(a) whilst the solid lines represent the predicted motion using single Newtonian viscosities of 97.7 Pa s (the low-shear viscosity) and 13 Pa s (the derived equivalent viscosity), respectively.

by Davis *et al.* (2002). Rather, we believe that this small apparent rebound may be due to the effects of fluid compressibility or viscoelasticity.

By examining data for the instantaneous velocities for this data set, in figure 6(b), we see similar qualitative trends as figure 3(d) for the lower viscosity Newtonian film. However, by examining only the data for $v(t) \geqslant 0$, as shown in figure 7(a), we can provide a fit to the data using (3.1). Here, we have used regression to determine the 'apparent' viscosities which provide the best fit to the data – in this case, for the low impact velocities, $v_0 = 0.53$ and 0.81 m s^{-1}, the viscosity which best fits the data is $\mu = 22$ Pa s whereas for the higher impact velocities, $u_i = 1.21$, 1.40 and 1.70 m s^{-1}, we conclude $\mu = 13$ Pa s. These apparent viscosities are far lower than the nominal low-shear value of $\mu = 97.7$ Pa s. To highlight the dramatic shear-thinning effect here, figure 7(b) plots the original trajectory of the sphere for $v_0 = 1.70$ m s^{-1} and the predicted motions using both the low-shear viscosity stated by the manufacturer and the projected viscosity derived from (3.1). The trajectory from the low-shear viscosity of 97.7 Pa s shows strong deviation from the observed experimental trajectory from early times ($t \sim 0.4$ ms) and has reached its minimum separation distance, $x_{min} = 1.08$ mm, at $t \sim 4$ ms. In contrast, the trajectory for $\mu = 13$ Pa s penetrates to a minimum separation of $x_{min} = 8.3$ μm in a time of $t \sim 3$ ms. Although no single viscosity can truly describe the motion for this fluid, the lower viscosity of $\mu = 13$ Pa s clearly predicts the motion over the initial stages much more accurately.

From the rheological data given in figure 2, we can derive some effective viscosities based on the shear rate in the thin layer, approximated by $\dot{\gamma}_{exp} \sim u(t)/\Delta x(t)$. Near to the entry of the sphere and close to the surface of the glass plate, this corresponds to effective shear rates of $\dot{\gamma} \sim 8300$ and 9700 respectively, which translates to viscosities of 12.3 and 11.2 Pa s, which is very close to the value obtained from the fit provided by (3.1) in figure 7(a) of 13 Pa s.

The crude approach used to derive a Newtonian equivalent viscosity, however, does not take into account the true shearing effect in the fluid as the sphere travels

throughout the film. A better, quantitative examination of the flow-field in this geometry is sure to provide a more accurate description of the shear and extension which could then be used in calculation of effective viscosities at each time step. This is beyond the scope of the present work, but will be assessed in the future. As a first approximation, however, we propose that the fitting method used in figure 7 may be useful in determining the short-time dynamical behaviour of non-Newtonian fluids. In addition, the observations in figures 6 and 7 highlight the importance of using well-behaved liquids in lubrication experiments.

4. Conclusions

An experimental approach employing high-speed video imaging has been used to verify the lubrication force exerted on a sphere when penetrating through a thin viscous film covering a solid wall. The results for high-viscosity Newtonian fluids show excellent agreement with the theoretical trajectories computed from the equations of motion based on the lubrication force, $F_L = 6\pi\mu a^2 v/x$. The distance of closest approach determined experimentally when the velocity first reaches zero was shown to be in good agreement with theoretical predictions based on the threshold $F_L \leqslant mg$ when plotted against the impact Stokes number. Experiments performed with shear-thinning fluids show interesting behaviour where compressibility may be important and we propose that this simple experimental configuration can be used to provide insight into the short-time dynamical behaviour of non-Newtonian fluids which is otherwise difficult to determine.

REFERENCES

AMBARI, A., GAUTHIER-MANUEL, B. & GUYON, E. 1984 *J. Fluid Mech.* **149**, 235–253.

BARNOCKY, G. & DAVIS, R. H. 1988 *Phys. Fluids* **31(6)**, 1324–1329.

BRENNER, H. 1961 *Chem. Engng Sci.* **16**, 242–251.

COX, R. E. & BRENNER, H. 1967 *Chem. Engng Sci.* **22**, 1753–1777.

DAVIS, R. H., RAGER, D. A. & GOOD, B. T. 2002 *J. Fluid Mech.* **468**, 107–119.

DAVIS, R. H., SERAYSSOL, J.-M. & HINCH, E. J. 1986 *J. Fluid Mech.* **163**, 479–497.

DONAHUE, C. M., HRENYA, C. M., DAVIS, R. H., NAKAGAWA, K. J., ZELINSKAYA, A. P. & JOSEPH, G. G. 2010 *J. Fluid Mech.* **650**, 479–504.

GONDRET, P., HALLOUIN, E., LANCE, M. & PETIT, L. 1999 *Phys. Fluids* **11** (9), 2803–2805.

GONDRET, P., LANCE, M. & PETIT, L. 2002 *Phys. Fluids* **14** (2), 643–652.

KANTAK, A. A., HRENYA, C. M. & DAVIS, R. H. 2009 *Phys. Fluids* **21**, 023301.

LIAN, G., ADAMS, M. J. & THORNTON, C. 1996 *J. Fluid Mech.* **311**, 141–152.

SALMAN, A. D., HOUNSLOW, M. J. & SEVILLE, J. P. K. (Ed.) 2006 *Handbook of Powder Technology, Vol.11: Granulation.* Elsevier Science.

THORODDSEN, S. T., ETOH, T. G. & TAKEHARA, K. 2008 *Annu. Rev. Fluid Mech.* **40**, 257–285.